

Peroxodiiron Complexes of Polypyridine Ligands: Syntheses, Physicochemical Properties, and Thermal Stability Markedly Enhanced by Hexapyridine Dinucleating Ligand

Masahito Kodera,* Motoharu Itoh, Koji Kano, and Takuzo Funabiki

Department of Molecular Science and Technology, Doshisha University, Kyotanabe, Kyoto 610-0321

Received May 24, 2005; E-mail: mkodera@mail.doshisha.ac.jp

The peroxodiiron(III) complexes $[Fe_2(O)(O_2)(OAc)(hexpy)](CF_3SO_3)$ (**2**) and $[Fe_2(O)(O_2)(OAc)(tripy)_2](ClO_4)$ (**4**) (hexpy = 1,2-di[6-bis(2-pyridyl)methyl-2-pyridyl]ethane and tripy = 2-di(2-pyridyl)methyl-6-methylpyridine) were prepared by addition of H_2O_2 to the di(μ-acetato)-μ-oxodiiron(III) complexes $[Fe_2(O)(OAc)_2(hexpy)](CF_3SO_3)_2$ (**1c**) and $[Fe_2(O)(OAc)_2(tripy)_2](ClO_4)_2$ (**3**) in MeCN, respectively. The peroxo complex **2** was isolated as a purple solid, but **4** could not be due to its instability. Detailed spectral studies of **2** and **4** revealed the unique triply bridged μ-acetato-μ-oxo-μ-1,2-peroxodiiron(III) core structures. The spontaneous decomposition of **2** and **4** in various solvent systems was kinetically investigated. The half-life of **2** and **4** in dry MeCN was 8.7 h at 300 K and 10 min at 263 K, respectively, clearly showing that the thermal stability of **2** is markedly enhanced by the hexpy ligand.

The diiron–dioxygen chemistry of non-heme diiron proteins[1,2] such as hemerythrin[3–10] and soluble methane monooxygenase (sMMO)[11–25] has attracted the interest of chemists and biochemists given the unique mechanisms of reversible O_2-binding[3–6] and O_2-activation.[11–16] Structural and spectroscopic studies concerning non-heme diiron proteins[8–11,17–24] and their excellent model systems has contributed towards our understanding of the mechanisms of diiron–dioxygen chemistry[26–47] and facilitated the development of efficient biomimetic oxidation catalysts.[48–53] However, mechanistic studies employing native proteins remain problematic due to the instability of the peroxodiiron intermediates and the active species. Thus, thermally stable peroxodiiron(III) complexes have been employed as useful functional models.[26–33] A variety of peroxodiiron(III) complexes have been synthesized containing sterically hindered ligands.[27–33] Examples of sterically hindered ligands are shown in Chart 1. To date, investigations concerning O_2-activation with peroxodiiron(III) complexes have been sparse.

We previously developed a series of polypyridine ligands[54] consisting of the tripyridine tridentate ligand 2-di(2-pyridyl)-methyl-6-methylpyridine (tripy), and the hexapyridine dinucleating hexadentate ligand 1,2-bis[6-di(2-pyridyl)methyl-2-pyridyl]ethane (hexpy).[55] The chemical structure of the tripy and hexpy ligands are shown in Scheme 1. The hexpy ligand is an excellent dinucleating ligand, which possesses two tris(2-pyridyl)methane moieties connected by a $-CH_2CH_2-$ tether, that can specifically stabilize the dinuclear structure of various metal complexes in the solid state and in solution.[26,52,54–57] We reported that diiron(III) complexes of the hexpy ligand $[Fe_2(O)(OAc)_2(hexpy)](X)_2$ [X = ClO_4 (**1a**), PF_6 (**1b**), and CF_3SO_3 (**1c**)] and a diiron(III) complex of the tripy ligand $[Fe_2(O)(OAc)_2(tripy)_2](ClO_4)_2$ (**3**) are useful as functional models of non-heme diiron proteins.[55] The diiron complexes of the hexpy ligand are stable in solution, though the diiron complex of the tripy ligand is gradually converted to a mononuclear bis-ligand complex in polar solvents.[55] The hexpy ligand does not possess a large steric hindrance. This leads to the efficient catalysis by **1** of the hydroxylation of alkanes with *m*-chloroperbenzoic acid where the catalytic turnover number was shown to exceed one thousand.[52]

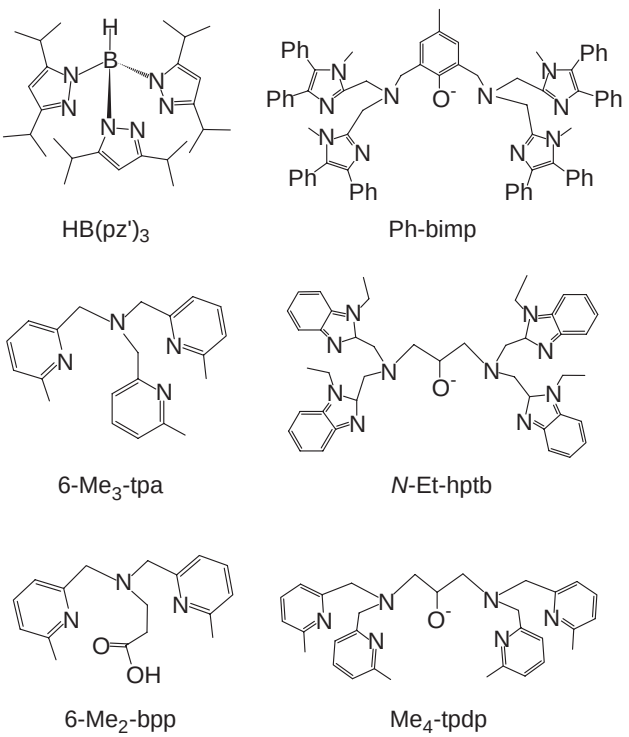

Chart 1.

We recently found that the hexpy ligand could form the thermally stable peroxodiiron(III) complex $[Fe_2(O)(O_2)(OAc)(hexpy)](CF_3SO_3)$ (**2**).[26] Here, we report on the syntheses and

Published on the web February 10, 2006; DOI 10.1246/bcsj.79.252

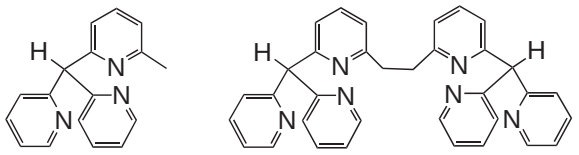

Scheme 1.

physicochemical properties of the peroxodiiron(III) complexes of hexpy and tripy, $[Fe_2(O)(O_2)(OAc)(hexpy)](CF_3SO_3)$ (**2**) and $[Fe_2(O)(O_2)(OAc)(tripy)_2](ClO_4)$ (**4**), and show that **2** is much more stable than **4**, although the μ-acetato-μ-oxo-μ-peroxodiiron(III) core structures of **2** and **4** resemble one another. The marked thermal stability of **2** might be due to the dinucleating effect of the hexpy ligand.

Experimental

Materials. All ordinary reagents and solvents were purchased and used as received unless otherwise noted. MeCN was dried over P_2O_5 and distilled. CH_2Cl_2 was dried over anhydrous CaO and distilled. $H_2{}^{18}O_2$ was prepared according to a previously described procedure.[58] The polypyridine ligands 2-di(2-pyridyl)methyl-6-methylpyridine (tripy) and 1,2-bis[6-di(2-pyridyl)methyl-2-pyridyl]ethane (hexpy), and the diiron(III) complex of the tripy ligand $[Fe_2(O)(OAc)_2(tripy)_2](ClO_4)_2$ (**3**) were prepared according to previously described procedures.[55]

Measurements. Elemental analyses (C, H, and N) were carried out at the Elemental Analysis Service Center of Kyoto University. The amount of iron was determined using a Shimadzu AA-610 atomic absorption/flame emission spectrophotometer. UV–vis absorption spectra were recorded on a Hitachi U-3210 spectrophotometer and an Oothuka Photal MCPD-7000 MM. Infrared (IR) spectra were taken on a Shimadzu FT-IR-8400 spectrometer using KBr disks or NaCl plates. Fast atom bombardment (FAB) mass spectra were obtained on a JEOL JMS-DX 300 spectrometer using *m*-nitrobenzylalcohol (NBA) as a matrix. A cold spray ionization (CSI) mass spectrum was obtained on a JEOL JMS-T100CS spectrometer in MeCN at $-30\,^{\circ}C$. ^1H NMR spectra of the diiron complexes in CD_3CN were recorded on a JEOL JMN-A 400 spectrometer using Me_4Si as an internal standard. ESR spectra were recorded on a JEOL JES-TE200 spectrometer in MeCN or MeCN–CH_2Cl_2 at 77 K. Magnetic susceptibilities were measured on a Quantum Design MPMS2 XL SQUID susceptometer in the temperature range 2–300 K. Mössbauer spectra were measured at the National Institute of Bioscience and Human-Technology at Tsukuba. The radioactive source was ^{57}Co(Rh). Isomer shifts were reported relative to metallic iron foil. Resonance Raman (RR) scattering was excited at 592.7 and 647.1 nm using an Ar-dye-laser and detected with a CCD detector (Princeton Instruments) attached to a single polychromator. All measurements were carried out at $-30\,^{\circ}C$ using a spinning cell. Raman shifts were calibrated with acetone, and the accuracy of the peak positions of the Raman bands was $\pm 1\,cm^{-1}$.

Preparations. $[Fe_2(O)(OAc)_2(hexpy)](CF_3SO_3)_2$ (1c): 250 mg (0.48 mmol) of hexpy was added to a suspension of 331 mg (0.55 mmol) of $Fe_3Cl(O)(OAc)_6\cdot 3H_2O$ in 10 mL of EtOH, and the mixture was stirred at room temperature for 12 h. To the resultant solution was added 412 mg of CF_3SO_3Na, and **1c** precipitated as a brown solid. After 4 h of stirring, the brown solid was collected by filtration, washed with EtOH and dried in vacuo. **1c** was purified by recrystallization from CH_2Cl_2/MeCN/Et_2O. The yield of **1c** was 322 mg (yield 63%). Anal. Calcd for **1c**$\cdot 1/2CH_2Cl_2$ ($C_{40.5}H_{35}N_6Fe_2F_6O_{11}S_2Cl$): C, 43.94; H, 3.19; N, 7.59; Fe, 10.09%. Found: C, 44.03; H, 3.16; N, 7.79; Fe, 10.27%. IR (KBr disk) (ν_{max}/cm^{-1}): 3050 (aromatic C–H), 1600, 1560, 1530, 1470, 1440 (py ring), 1440 (acetato), 1275, 1250, 1220, 1030 (CF_3SO_3), 740 (Fe–O–Fe). ^1H NMR [CD_3CN, 25 °C, δ, ppm (TMS)]: 7.74, 8.03, 8.50, 11.39, 12.90, and 15.08. FAB mass data: m/z 915 $[M]^+$ and 856 $[M - OAc]^+$.

$[Fe_2(O)(O_2)(OAc)(hexpy)](CF_3SO_3)$ (2): To a solution of **1c** (38 mg, 0.033 mmol) in MeCN (10 mL) was added 10 µL of Et_3N (0.072 mmol) and 100 µL of 20% H_2O_2/MeCN (0.50 mmol of H_2O_2) at 0 °C. The mixture was stirred at 0 °C and gradually turned dark purple. The reaction was monitored by inspection of the electronic absorption spectra measured using an aliquot taken from the reaction mixture. Following completion of the reaction, the reaction mixture was concentrated to 2 mL under reduced pressure at low temperature. To the residue was added 10 mL of dry Et_2O at low temperature and **2** precipitated as a purple solid. The supernatant was decanted and the purple solid was washed with dry Et_2O. After the washing/decantation cycle was repeated several times, the purple solid was collected by filtration and dried in vacuo. 36 mg of **2** was isolated (yield 95%). Anal. Calcd for $C_{37}H_{41}F_3Fe_2N_6O_{13}S$: C, 45.42; H, 4.22; N, 8.59; Fe, 11.41%. Found: C, 46.59; H, 3.80; N, 8.48; Fe, 12.14%. ^1H NMR [CD_3CN, −30 °C, δ, ppm (TMS)]: 1.10, 4.09, 7.38, 7.59, 8.12, 8.73, 10.12, 10.61, 11.13, 11.24, 12.91, and 14.75. ESR: silent in MeCN at 77 K.

$[Fe_2(O)(O_2)(OAc)(tripy)_2](ClO_4)$ (4): To a solution of **3** (9.4 mg, 0.01 mmol) in MeCN (10 mL) was added 10 µL of 20% H_2O_2/MeCN (0.05 mmol of H_2O_2) at −30 °C. The mixture was stirred for several minutes and turned dark purple. Complete formation of the peroxodiiron(III) complex **4** was confirmed by monitoring the change in the electronic absorption spectrum. **4** could not be isolated due to thermal instability and was used for the spectral measurements as prepared without purification. ESR: silent in MeCN at 77 K.

Kinetic Measurements for the Spontaneous Decomposition of 2 and 4. For the kinetic measurements, solutions of **2** (3×10^{-4} M) were freshly prepared by dissolving the isolated solid in various solvent systems including dry MeCN, dry MeCN/CH_2Cl_2 (1:3, v/v), or MeCN in the presence of H_2O (0.28, 1.11, 1.67, and 2.22 M), and then quickly degassing the mixture by employing several cycles of evacuation and refilling using Ar. A typical method used for the kinetic measurements was as follows. A solution (2 mL) of **2** was placed in a quartz-cell under anaerobic conditions and the temperature maintained at 300 ± 0.2 K during the measurements. The decrease in **2** was monitored at 605 nm. The first-order rate constants (k_{obs}) were obtained from fits of $-\ln(1 - A_t/A_\infty)$ vs time. Plots of the kinetic data gave straight lines for each kinetic measurement. The kinetic measurements were also carried out using different concentrations of **2** (2.0–10.0×10^{-4} M).

4 was prepared upon addition of 5 equiv of 10% H_2O_2/MeCN to a solution of **3** (3×10^{-4} M) in MeCN at 243 K under Ar, and used for the kinetic studies without purification. The kinetic measurements of **4** were carried out at 263 K using almost the same method as described above for **2**. The kinetic measurements were also carried out at different concentrations of **4** (2.0–13.0×10^{-4} M).

Product Analysis for the Spontaneous Decomposition of 2. After the solution of **2** in MeCN was allowed to stand for 12 h at room temperature, the solution was concentrated to dryness. The electronic absorption, ^1H NMR, and FAB-MS spectra of the

resultant products were measured. Moreover, to investigate the ligand structure, the metal-free ligand was obtained as follows. To the residue was added CH_2Cl_2 and an aqueous solution of EDTA. The mixture was stirred for 12 h, the CH_2Cl_2 layer was separated and the aqueous layer was extracted with CH_2Cl_2. The CH_2Cl_2 layers were combined and concentrated to dryness to yield the metal-free ligand mixture. The metal-free ligand mixtures were examined by ^{1}H NMR, which showed that 96% of hexpy was recovered from the spontaneous decomposition of **2** under Ar, while 77% of hexpy was recovered from that under O_2. The FAB-MS spectrum of the metal-free ligand mixture shows a main peak at m/z 521, corresponding to $[L + H]^+$ and only a minor peak at m/z 537, corresponding to $[L + O + H]^+$.

Determination of H_2O Contained in Dry MeCN. The titration using a Karl Fischer reagent was carried out in a glove box under a N_2 atmosphere. As a color standard, a solution of I_2 (25.4 mg) in dry MeOH (10 mL) was prepared. The Karl Fischer reagent was place in a volumetric dropping funnel and added to 100 mL of dry MeOH until the solution turned the same brown color as the color standard. To the mixture was added 10 mL of dry MeCN and the solution turned yellow. The yellow solution was titrated with the Karl Fischer reagent until the solution turned brown. The concentration of H_2O contained in the dry MeCN used for the various measurements as a solvent was determined to be 4×10^{-3} M.

Crystal Structure Analysis. Crystals of **3** suitable for X-ray analysis were obtained by slow diffusion of Et_2O to a solution of **3** in CH_2Cl_2–MeCN at room temperature. A crystal with approximate dimensions of $0.1 \times 0.2 \times 0.5$ mm^3 was sealed in a glass capillary and used for the X-ray diffraction analysis. Measurements were performed on a Rigaku AFC7R/CCD diffractometer with graphite monochromated Mo Kα radiation ($\lambda = 0.71069$) and a 12 kW rotating anode generator. The data were collected at 293 ± 1 K to a maximum 2θ value of 55.0°. The crystal-to-detector distance was 35.12 mm, and the detector swing angle was 10.04°. A total of 23807 reflections were collected of which 5288 were unique ($R_{int} = 0.096$).

The structure was solved by a direct method (SIR 2002) and expanded using Fourier techniques. Some non-hydrogen atoms were refined anisotropically, while the rest were refined isotropically. Hydrogen atoms were refined using the riding model. The final cycle of full-matrix least-squares refinement was based on 1893 observed reflections ($I > 3.00\sigma(I)$) and 270 variable parameters. The neutral atom scattering factors were taken from Cromer and Waber.[59] Anomalous dispersion effects were included in F_c,[60] the values for $\Delta f'$ and $\Delta f''$ being taken from the reference[61] and those of Creagh and McAuley.[61] Calculations were performed using the Crystal Structure Crystallographic software package.[62] Crystal parameters and important data collection for **3** are summarized in Table 1. Crystallographic data has been deposited with Cambridge Crystallographic Data Centre: Deposition number CCDC-274092 for **3**. Copies of the data can be obtained free of charge via http://www.ccdc.cam.ac.uk/conts/retrieving.html (or from the Cambridge Crystallographic Data Centre, 12, Union Road, Cambridge, CB2 1EZ, UK; Fax: +44 1223 336033; E-mail: deposit@ccdc.cam.ac.uk).

Results and Discussion

Comparison of the Crystal Structure of $[Fe_2(O)(OAc)_2(hexpy)](ClO_4)_2$ (1a) and $[Fe_2(O)(OAc)_2(tripy)_2](ClO_4)_2$ (3). The crystal structure of **1a** was previously reported.[55] The ORTEP view of the cation of **3**, $[Fe_2(O)(OAc)_2(tripy)_2]^{2+}$, is shown in Fig. 1 together with the numbering scheme. The cation lies on a crystallographic 2-fold axis and, accordingly, has exact 2-fold symmetry. The μ-oxo O-atom lies on the 2-fold axis. Each iron atom is coordinated by one O-atom of the μ-oxo bridge, two O-atoms of the μ-acetato bridges and three N-atoms of the tripy ligand in a distorted octahedral geometry. The selected bond distances and angles of **3** are summarized in

Table 1. Crystallograpic Data for **3**

	3
Empirical formula	$C_{19}H_{18}Cl_1Fe_1N_3O_{6.5}$
Formula weight	483.67
Crystal system	monoclinic
Space group	$C2/c$ (No. 15)
a/Å	21.154(8)
b/Å	12.388(4)
c/Å	20.573(8)
β/deg	120.040(7)
V/Å^3	4667.3(29)
Z	8
T/°C	20.0
D_{calcd}/g cm^{-1}	1.377
Radiation/Å	Mo Kα ($\lambda = 0.71070$)
μ/cm^{-1}	7.99
R,[a] Rw[b]	0.088, 0.131
Goodness of fit indicator	0.924

a) $R = \Sigma||F_o| - |F_c||/\Sigma|F_o|$. b) $Rw = [\Sigma w(|F_o| - |F_c|)^2/\Sigma w(F_o)^2]^{1/2}$, $w = 1/[0.0178(F_o)^2 + 1.00\sigma(F_o^2)]$.

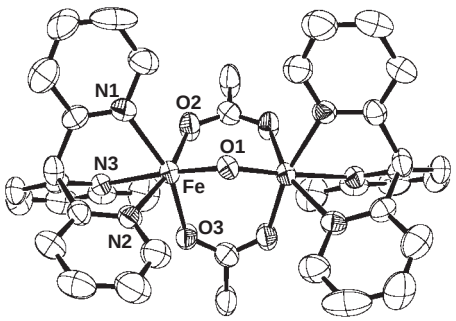

Fig. 1. ORTEP diagram the cationic portion of **3**.

Table 2. Selected Bond Distances (Å) and Angles (deg) for **3**

3					
Bond Distances					
Fe···Fe′	3.162(2)				
Fe–O(1)	1.810(6)	Fe–O(2)	2.019(9)	Fe–O(3)	2.01(1)
Fe–N(1)	2.17(1)	Fe–N(2)	2.159(9)	Fe–N(3)	2.32(1)
Bond Angles					
O(1)–Fe–O(2)	95.3(3)	O(1)–Fe–O(3)	95.2(3)		
O(1)–Fe–N(1)	103.8(3)	O(1)–Fe–N(2)	94.6(4)		
O(1)–Fe–N(3)	175.4(3)	O(2)–Fe–O(3)	99.4(4)		
O(2)–Fe–N(1)	86.9(4)	O(2)–Fe–N(2)	167.2(4)		
O(2)–Fe–N(3)	86.0(3)	O(3)–Fe–N(1)	159.4(3)		
O(3)–Fe–N(2)	87.8(4)	O(3)–Fe–N(3)	80.3(4)		
N(1)–Fe–N(2)	82.8(4)	N(1)–Fe–N(3)	80.6(4)		
N(2)–Fe–N(3)	84.8(4)	Fe–O(1)–Fe′	121.7(6)		

Table 3. Structural Data of Diiron(III) Cores of **1a**, **3**, and the Related Compounds

	1a	**3**	$HB(pz)_3$[a]	Me_3tacn[b]
Fe···Fe′/Å	3.142(3)	3.162(2)	3.146(1)	3.12(4)
Fe–O_{oxo}/Å	1.782(5)	1.810(6)	1.788(2)	1.800(3)
			1.780(2)	
Fe–O_{AcO}(av)/Å	2.051(8)	2.015(9)	2.042(9)	2.034(3)
Fe–$N_{cis\ to\ \mu\text{-}oxo}$(av)/Å	2.192(9)	2.165(9)	2.153(3)	2.198(4)
Fe–$N_{trans\ to\ \mu\text{-}oxo}$/Å	2.209(9)	2.32(1)	2.188(3)	2.268(6)
Fe–O–Fe′/deg	123.6(6)	121.7(6)	123.6(1)	119.7(1)

a) $HB(pz)_3$ = $[Fe_2(O)(OAc)_2(HB(pz)_3)_2]$, b) Me_3tacn = $[Fe_2(O)(OAc)_2(Me_3tacn)_2]^{2+}$.

Table 2 together with comparable data for **1a**.[55] The structural features of the diiron cores of **1a** and **3** are summarized in Table 3 together with comparable data for the diiron(III) complexes of the general formula $[Fe_2(O)(OAc)_2(L)_2]^{2+}$ (L = $HB(pz)_3$ and Me_3tacn).[63,64]

The clear structural difference between **1a** and **3** is reflected in the position of the $–CH_2CH_2–$ tether group of the hexpy ligand and the 6-Me groups of the tripy ligands. The N-atoms of the 6-Mepy groups coordinate to the Fe atoms at the trans positions of the μ-O bridge in **3**. Thus, the 6-Me groups are located at the narrow side of the $Fe_2(\mu\text{-}OAc)_2$ core, opposite against the μ-O bridge, where the steric repulsion of the 6-Me groups may be minimized. The Fe–N(3) bond length of 2.32(1) Å is larger than the average value, 2.165(9) Å, of the Fe–N(1) and Fe–N(2) bond lengths in **3**, and also larger than the Fe–N(3) bond length, 2.209(9) Å, in **1a**. These data clearly show that the Fe–N(3) bond length of **3** is elongated by the steric repulsion of the 6-Me group. The tether group lies on the $Fe_2(\mu\text{-}O)(\mu\text{-}OAc)$ moiety in **1a**. The position of the tether group might be due to the length of the $–CH_2CH_2–$ chain. In contrast to **3**, the Fe–N bond lengths, 2.196(9), 2.188(9), and 2.209(9) Å, in **1a** are similar to each other. Thus, steric repulsion by the tether group has less of an influence on the bond lengths than that induced by the 6-Me groups.

Although the overall structure of the di(μ-acetato)-μ-oxodiiron(III) core of **1a** and **3** are similar, differences arising from the 6-Me and tether groups cause the distinguishable differences in the diiron cores. The Fe···Fe distance of 3.142(3) Å, the Fe–O(1) bond length of 1.782(5) Å, and the O(1)–Fe–N(1) angle of 93.9(3)° in **1a** are smaller than those in **3**, being 3.162(2) Å, 1.810(6) Å, and 103.8(3)°, respectively. The edge-to-edge distances between two tri(2-pyridyl)methane moieties in **1a** and **3** are 3.947 and 4.103 Å, respectively. Although the diiron core of **1a** apparently shrinks compared with that of **3**, the overall structural features of the diiron core of **1a**, as shown in Table 3, are closer to those of the di(μ-acetato)-μ-oxodiiron(III) complexes of $HB(pz)_3$ and Me_3tacn than those of **3**.[63,64] This indicates that the diiron core of **3** is more distorted than that of **1a**. Thus, unlike the tether group, the 6-Me groups induce distortion of the diiron core structure. Therefore, it can be said that the structure of the hexpy ligand, where the $–CH_2CH_2–$ tether connects two tri(2-pyridyl)methane moieties at the 6-position of the py groups, is most suitable for encapsulating the di(μ-acetato)-μ-oxodiiron(III) core.

Syntheses and Physicochemical Properties of Peroxodiiron(III) Complexes $[Fe_2(O)(O_2)(OAc)(hexpy)](CF_3SO_3)$ (2) and $[Fe_2(O)(O_2)(OAc)(tripy)_2](ClO_4)$ (4). The peroxodiiron(III) complex **2** was synthesized by reaction of **1c** with H_2O_2 in the presence of 2.2 equiv of Et_3N in MeCN, and was isolated as a purple solid given that it is stable at room temperature in the solid state. The elemental analysis using the isolated solid of **2** agreed with the formula $[Fe_2(O)(O_2)(OAc)(hexpy)](CF_3SO_3)\cdot 5H_2O$. The peroxodiiron(III) complex **4** was generated by addition of 5 equiv of H_2O_2 to a solution of **3** in MeCN at −30 °C just before use in various spectral studies. For the preparation of **4**, use of Et_3N was unnecessary.

The CSI-MS spectra of **2** and **4** in MeCN are shown in Fig. 2. **2** exhibits a major peak at m/z 739, corresponding to $[Fe_2(O)(O_2)(OAc)(hexpy)]^+$, consistent with the molecular formula. The isotope intensity pattern of the major peak matches the calculated one. The major peak shifted to m/z 743 following ^{18}O-labelling with $H_2{}^{18}O_2$, demonstrating that the bound peroxide is involved in **2**. The CSI-MS spectrum of **4** shows a positive ion peak at m/z 741, corresponding to $[Fe_2(O)(O_2)(OAc)(tripy)_2]^+$, and the ion exhibited an isotope intensity pattern that matches the calculated one, suggesting that the molecular formula of **4** is $[Fe_2(O)(O_2)(OAc)(tripy)_2](ClO_4)$.

The UV–vis spectra of **2** and **4** in MeCN are shown in Fig. 3. **2** shows two absorption bands at 510 (ε = 1300 $M^{-1}\,cm^{-1}$) and 605 nm (ε = 1310 $M^{-1}\,cm^{-1}$). **4** shows two absorption bands at 510 (ε = 1270 $M^{-1}\,cm^{-1}$) and 660 nm (ε = 1370 $M^{-1}\,cm^{-1}$). These spectra are similar to that of the μ-oxo-μ-1,2-peroxodiiron(III) complex $[Fe_2(O_2)(O)(6\text{-}Me_3\text{-}tpa)_2](ClO_4)_2$ (**5**), which shows absorption bands at 494 (ε = 1100 $M^{-1}\,cm^{-1}$) and 648 nm (ε = 1200 $M^{-1}\,cm^{-1}$).[33] The higher energy bands at around 500 nm were tentatively assigned to μ-oxo to Fe^{3+} charge-transfer transitions since similar μ-oxo to Fe^{3+} charge-transfer bands were observed at 507 nm (ε = 710 $M^{-1}\,cm^{-1}$), 500 nm (ε = 830 $M^{-1}\,cm^{-1}$), 492 nm (ε = 460 $M^{-1}\,cm^{-1}$), and 519 nm (ε = 600 $M^{-1}\,cm^{-1}$) for **1c**, **3**, and the di(μ-acetato)-μ-oxodiiron(III) complexes of $HB(pz)_3$ and Me_3tacn, respectively.[62,63] It is noteworthy that the μ-oxo to Fe^{3+} charge-transfer bands were not strongly influenced by the different ligands. The lower energy bands at 605 and 660 nm may be assigned to the μ-peroxo to Fe^{3+} charge-transfer transitions. The μ-peroxo to Fe^{3+} charge-transfer band of **2** appeared at the higher energy side by 55 nm compared with that of **4**. This suggested that the Fe–O_{peroxo} bond is specifically stabilized by the hexpy ligand.

The resonance Raman spectrum of **2** is shown in Fig. 4. The spectrum shows two bands at 816 and 472 cm^{-1}, which shifted to 771 and 455 cm^{-1}, respectively, when **2** was labeled with $H_2{}^{18}O_2$. These two ^{18}O-sensitive bands are respectively assigned to the $\nu_{O\text{–}O}$ and $\nu_{Fe\text{–}O}$ of the bound peroxide. The resonance Raman spectrum of **4** shows a band at 856 cm^{-1}, being in the range of 848–900 cm^{-1} reported for (μ-1,2-peroxo)diiron(III) complexes,[27–45] and assignable to the $\nu_{O\text{–}O}$ of the bound peroxide. The $\nu_{O\text{–}O}$ value of **2** is notably below the range of the reported $\nu_{O\text{–}O}$ bands, 848–900 cm^{-1}. It was reported that the $\nu_{O\text{–}O}$ value is mainly dependent on the Fe–O–O angle of the peroxodiiron(III) complex.[34] The reason why **2** may have smaller Fe–O–O angles than the known complexes is that the hexpy dinucleating ligand encapsulates the diiron

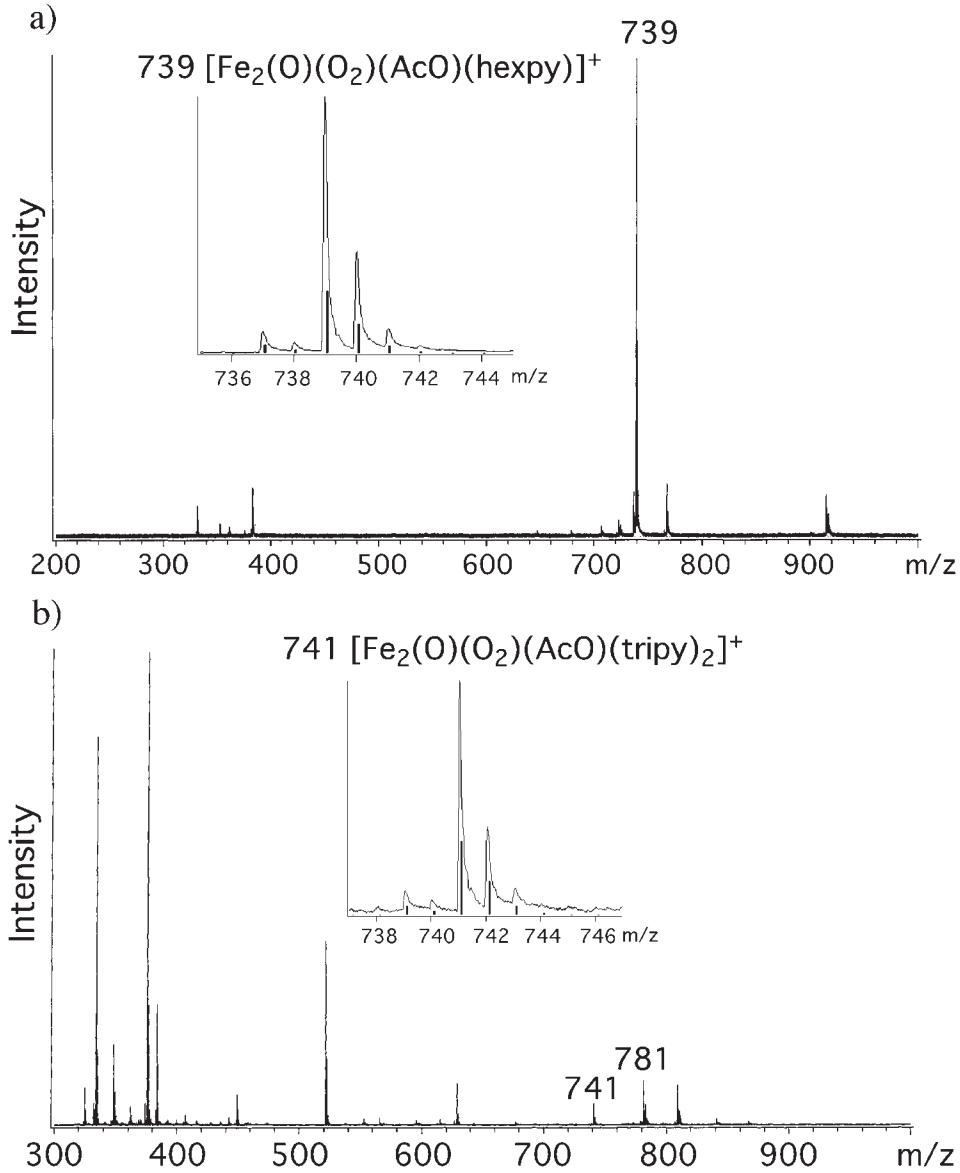

Fig. 2. CSI-MS spectra of **2** a) and **4** b) in MeCN at room temperature. The isotope patterns of $[Fe_2(O)(O_2)(OAc)(hexpy)]^+$ and $[Fe_2(O)(O_2)(OAc)(tripy)_2]^+$ shown in the spectra.

core to decrease the Fe···Fe distance. This is consistent with the structural features of **1a**, where the hexpy ligand decreases the Fe···Fe distance by encapsulating the diiron core.

The Mössbauer spectrum of **2** at 4.2 K is shown in Fig. 5 and shows only a quadrupole doublet with $\Delta E_Q = 1.67(8)$ mm/s and $\delta = 0.53(8)$ mm/s, indicating that the high-spin diiron(III) unit is symmetrically bridged by the peroxide. These values are close to the $\Delta E_Q = 1.68$ mm/s and $\delta = 0.54$ mm/s of the peroxodiiron(III) complex **5**,[33] and $\Delta E_Q = 1.79$ mm/s and $\delta = 0.52$ mm/s of $[Fe_2(O_2)(OBz)_2\{HB(pz'_3\}_2]$ (**6**).[29,34,65]

The cryomagnetic properties of **2** are represented in Fig. 6 by a plot of χ_M vs T in the temperature range 4–300 K. The magnetic susceptibility decreases with decreasing temperature. The exchange-coupling constant (J) of **2** was determined from the temperature dependent magnetic susceptibility data. An excellent fit of the χ_M–T data to a dinuclear model is obtained when $J = -55\,cm^{-1}$, $g = 2.00$, and paramagnetic impurity (%) = 0.007 are assumed for **2**. The result indicates strong antiferromagnetic spin-coupling between a pair of Fe(III) ions. The magnetic interaction in **2** is much stronger than that in **6** ($J = -33\,cm^{-1}$).[34] The μ-oxo bridge in **2** strengthens the magnetic interaction between the Fe(III) ions.

All these data show that the diiron center of **2** and **4** is triply bridged by the acetate, oxide, and peroxide anions to form the μ-acetato-μ-oxo-μ-1,2-peroxodiiron core. The proposed structure of **2** is shown in Fig. 7. The bridging modes known for triply bridged peroxodiiron(III) complexes are (1) μ-alkoxo-μ-carboxylato-μ-1,2-peroxo, (2) μ-carboxylato-μ-1,2-peroxo-μ-phenolato, and (3) di(μ-carboxylato)-μ-1,2-peroxo. Thus, the bridging mode of **2** and **4** represents the first type. Moreover, it is noted that the μ-oxo bridge was found in the triply bridged peroxodiiron(III) complexes **2** and **4**, although the bridging groups of the doubly bridged peroxodiiron(III) complexes are almost μ-oxo and μ-peroxo. Therefore, the net charge of the diiron core of **2** and **4** is 1+. This is quite unique because the net charge of the diiron cores of per-

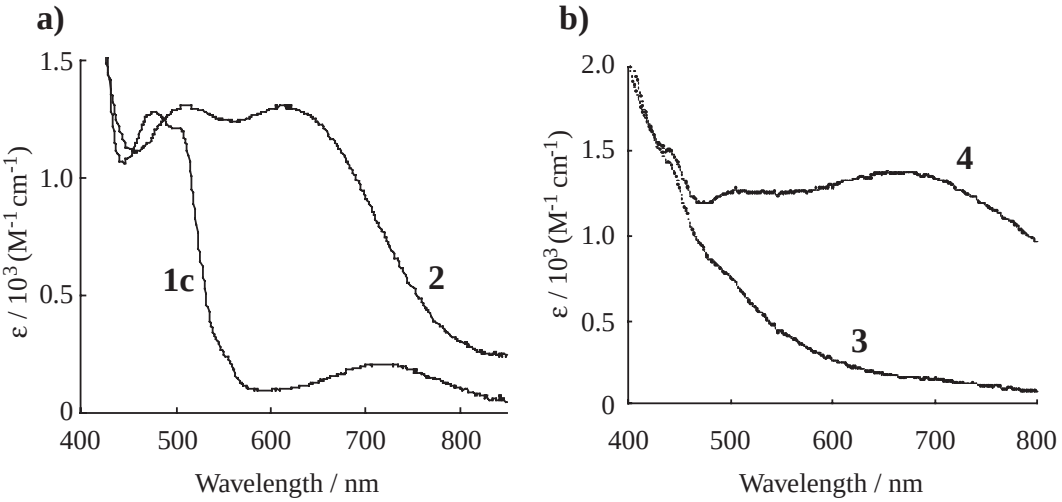

Fig. 3. a) UV–vis absorption spectra of **1c** and **2** in MeCN at room temperature. b) UV–vis absorption spectra of **4** generated from **3** upon addition of H_2O_2 in MeCN at −30 °C.

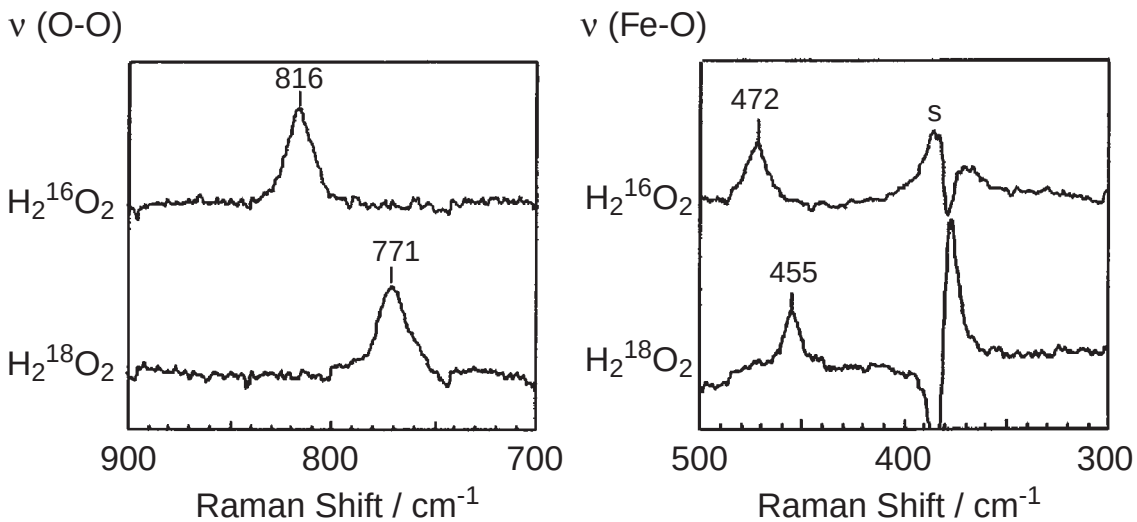

Fig. 4. Resonance Raman spectra of **2** (5×10^{-3} M) in MeCN at −30 °C with 592.7 nm (Ar-dye-laser) excitation.

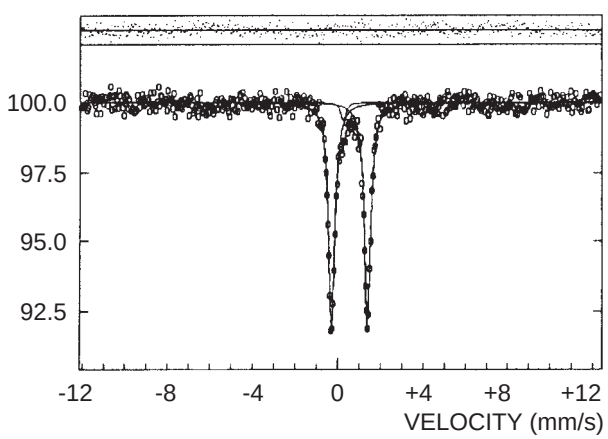

Fig. 5. Mössbauer spectrum of **2**. The spectrum was recorded at 4.2 K. The solid line is a simulated spectrum with ΔE_Q: 1.67(8) mm/s and δ: 0.53(8) mm/s.

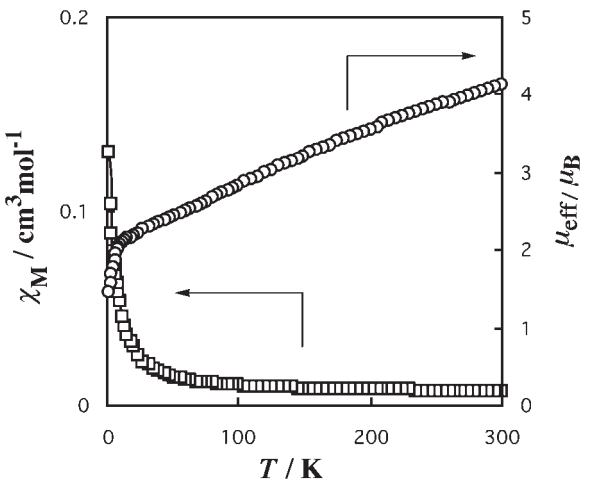

Fig. 6. Temperature dependence of magnetic susceptibility χ_M (□) and magnetic moment μ_{eff} (○) of **2**.

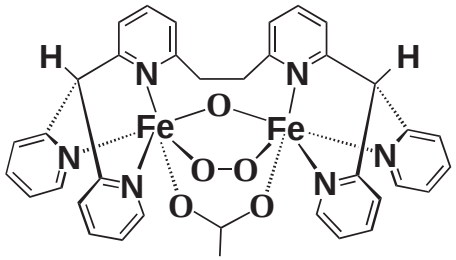

Fig. 7. Proposed structure of the cation portion of the peroxodiiron complex **2**.

oxodiiron(III) complexes known to date is 2+ or 3+. It is known that the tri(2-pyridyl)methane ligand, being the tridentate donor in the tripy and hexpy ligands, can stabilize the low-valence state of metal complexes. Thus, use of the polypyridine ligands tripy and hexpy might be suitable to lower the net charge of the diiron core due to the electronic character of the ligands in stabilizing the low-valence state.

Thermal Stability of 2 and 4. Excess H_2O_2 was not present in the solution of **2** because the solution was freshly prepared by dissolving the isolated solid. The decrease in **2** was monitored at 605 nm. The decay data obeyed good first-order kinetics as shown in Fig. 8. The first-order rate constant, $k = 2.2 \times 10^{-5}\,s^{-1}$ (half-life $\tau_{1/2} = 8.7\,h$), was obtained for the spontaneous decomposition of **2** in dry MeCN at 300 K. The kinetic measurements were also carried out using various concentrations of **2** ($2.0–10.0 \times 10^{-4}$ M) in dry MeCN. The results are shown in Fig. 8. The first-order rate constants are independent of the concentration of **2**, demonstrating that **2** decomposes unimolecularly in the concentration range employed ($2.0–10.0 \times 10^{-4}$ M).

The spontaneous decomposition of **2** was monitored by examination of the FAB-MS spectra, where the peak at m/z 707, corresponding to $[Fe_2(O)(OAc)(hexpy)]^+$, increased with the decrease in the peak at m/z 739, corresponding to $[Fe_2(O)(O_2)(OAc)(hexpy)]^+$. The decomposed products were also analyzed by examination of the ^{1}H NMR and electronic absorption spectra. The ^{1}H NMR and electronic absorption spectra of the decomposed product were similar to those of **1c**, indicating that the decomposed products mainly consisted of diiron(III) complexes similar to **1c**. Following demetallation of the decomposed products, the hexpy ligand was recovered almost quantitatively. Thus, oxygenation of the ligand did not occur during spontaneous decomposition. Even in the presence of an excess amount of cyclohexane as a substrate, oxygenated products of cyclohexane were not detected at all. Furthermore, we measured the spontaneous decomposition rate of **2** using MeCN-d_3 as a solvent, and the value of the kinetic isotope effect was 0.9. This value is close to 1 and is not reflective of a first-order kinetic isotope effect. These results suggested that O–O bond scission of the peroxo moiety of **2**, which must lead to oxygenation of the ligand, substrate or solvent, does not occur during spontaneous decomposition. Therefore, it might be suggested that the mechanism of spontaneous decomposition involves substitution of the peroxo ligand by a solvent molecule, so that O_2^{2-} and the decomposed diiron complexes would be generated, and O_2^{2-} would be protonated to H_2O_2. However, we were unable to detect any H_2O_2. The H_2O_2 might have decomposed via disproportionation catalyzed by the diiron complexes generated during spontaneous decomposition. The rate of disproportionation of H_2O_2 in such a reaction mixture must be much faster than the spontaneous decomposition of **2**, therefore, H_2O_2 does not accumulate to detectable levels.

The mixed solvent systems H_2O/MeCN ($[H_2O] = 0.28–2.22$ M) and CH_2Cl_2/MeCN (3:1, v/v) were used to investigate the solvent effect on the spontaneous decomposition of **2**. The concentration of remaining H_2O (4×10^{-3} M) in dry MeCN was determined by the Karl-Fischer method. This value is negligibly small compared with the concentration of H_2O in the mixed solvent system H_2O/MeCN. The dependence of the concentration of H_2O on the decomposition rate of **2** is shown in Fig. 9. The rate constants increased with increasing concentration of H_2O, with a y-axis intercept of $2.2 \times 10^{-5}\,s^{-1}$. The results show that the decomposition of **2** proceeds in the ab-

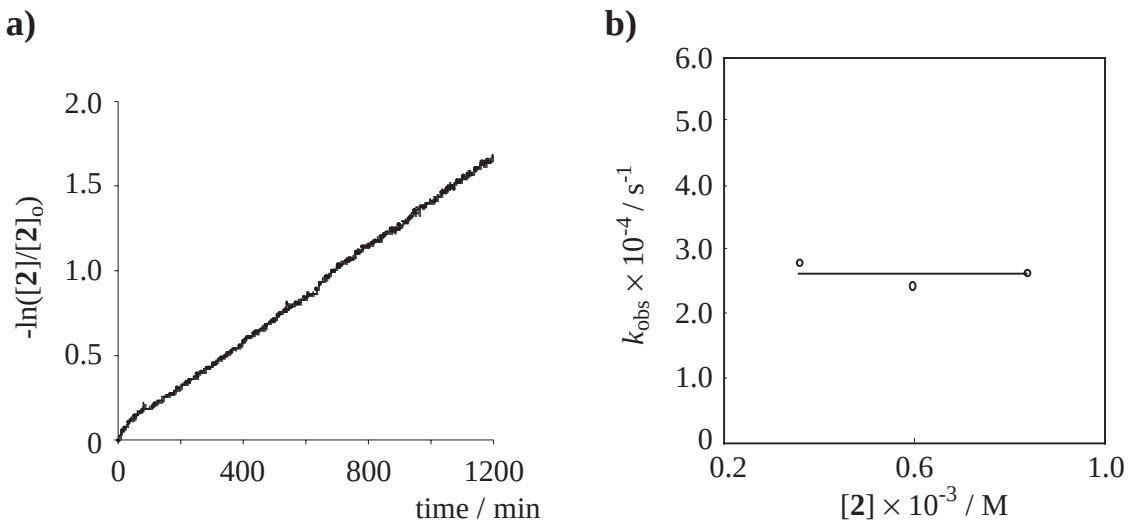

Fig. 8. a) The first-order plots for the spontaneous decomposition of **2** in MeCN at 300 K. b) The first-order rate constants at various concentrations of **2**, $[\mathbf{2}] = (2.0–10.0) \times 10^{-4}$ M in MeCN at 300 K.

sence of H_2O and is accelerated by the addition of H_2O. Thus, both MeCN and H_2O solvent molecules cause the decomposition of **2** independently. The rate constant, $8.0 \times 10^{-5}\,s^{-1}$, in H_2O/MeCN (1:9, v/v) is nearly four-fold larger than that in MeCN. Since the nucleophilicity of H_2O is stronger than that of MeCN, acceleration of the spontaneous decomposition of **2** in H_2O/MeCN (1:9, v/v) is mainly due to nucleophilic substitution of the peroxide by H_2O. The rate dependence of H_2O is not linear and seems to reflect a second-order dependence (see Fig. 9). The hydrogen bond of another H_2O molecule bound to peroxide may be involved in the acceleration. Although the effect of H_2O on the acceleration may be more complicated, the spontaneous decomposition of **2** might proceed via substitution of the peroxo moiety of **2** by MeCN or H_2O solvent molecules.

The half-life of **2** in more non-polar solvent systems such as CH_2Cl_2/MeCN (3:1, v/v) at 300 K increased to 20.3 h. This value is 2.3-fold larger than the 8.7 h half-life observed in dry MeCN. Nucleophilic substitution of bound peroxide by the solvent molecule must be retarded in such a non-polar solvent system. Thus, the stabilization of **2** in the non-polar solvent can be reasonably explained by the proposed decomposition mechanism: substitution of the bound peroxide by nucleophilic attack of the polar solvent. Therefore, it is concluded that spontaneous decomposition of **2** in various solvent systems proceeds via the substitution of bound peroxide by the polar solvent molecule to generate O_2^{2-} and diiron(III) complexes, and the H_2O_2 generated by protonation might be decomposed via disproportionation.

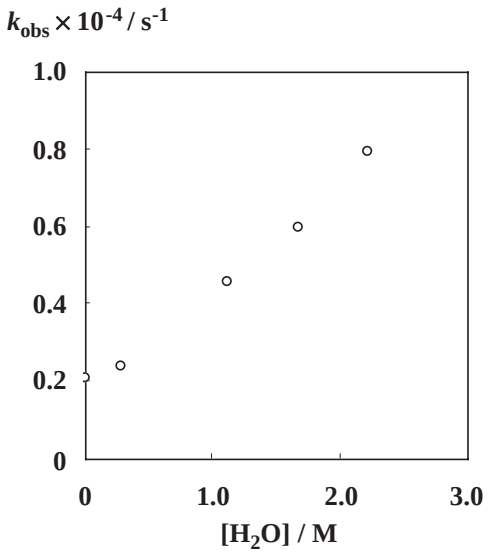

Fig. 9. The first-order rate constants at various concentrations of H_2O, $[\mathbf{2}] = 3.0 \times 10^{-4}$ M, $[H_2O] = (4 \times 10^{-3}$–2.22) M in MeCN at 300 K.

The spontaneous decomposition of **4** was monitored at 660 nm, and obeyed good first-order kinetics with $k = 1.1 \times 10^{-3}\,s^{-1}$ at 263 K in dry MeCN (half-life $\tau_{1/2} = 10$ min) (see Fig. 10). The half-life of **2** is much larger than that of **4**. Interestingly, **4** is slightly more stable than the doubly bridged μ-oxo-μ-1,2-peroxodiiron(III) complex $[Fe_2(O)(O_2)(6\text{-}Me_3\text{-}tpa)_2](ClO_4)_2$ (half-life 7.2 min at 243 K in MeCN).[33] The triply bridged structure of **4** might enhance the thermal stability. The concentration dependence on the decomposition rate of **4** is shown in Fig. 10. The rate constants are independent of the concentration of **4**. The bimolecular reaction of **4** is negligible in the spontaneous decomposition. The mechanism of the spontaneous decomposition of **4** might be similar to that of **2**, but more detailed kinetic studies and product analysis are necessary to clarify the decomposition mechanism of **4**.

As described above, **2** is thermally much more stable than **4**, although the triply bridged peroxodiiron core structure of **2** and **4** resemble one another. Thus, it can be said that the thermal stability of **2** is specifically enhanced by the hexpy ligand. As reflected in the crystal structure of **1a** and **3**, the structure of the hexpy ligand is most suitable for encapsulating the triply bridged diiron core. The diiron core of **1a** and **2** is $Fe_2(\mu\text{-}O)(\mu\text{-}OAc)_2$ and $Fe_2(\mu\text{-}O)(\mu\text{-}O_2)(\mu\text{-}OAc)$, respectively, which are similar except for the μ-OAc and μ-O_2 bridges. The μ-O_2 bridge, being composed of two atoms, may require a smaller

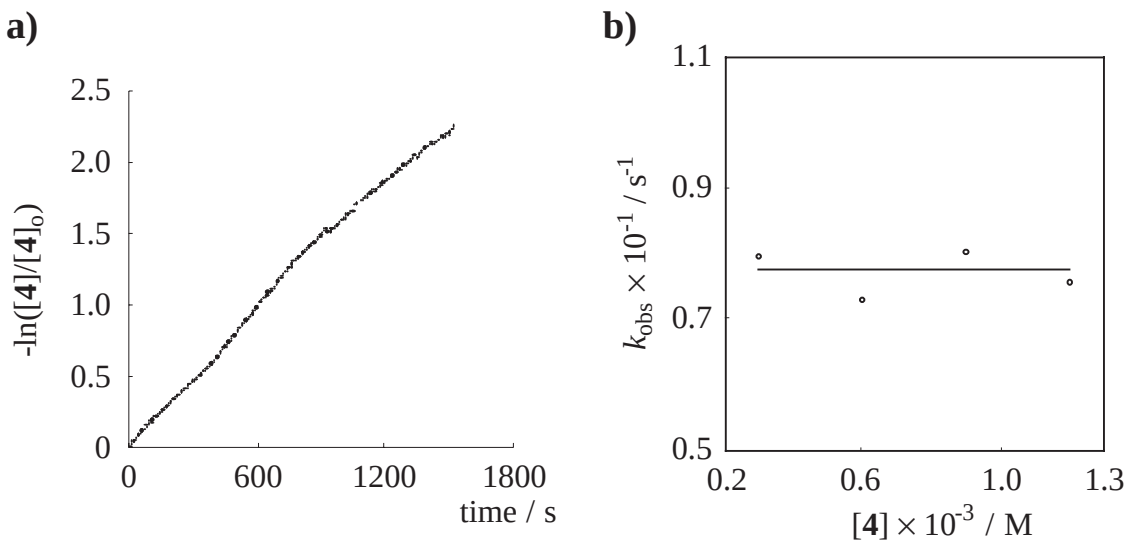

Fig. 10. a) The first-order plots for the spontaneous decomposition of **4** in MeCN at 263 K. b) The first-order rate constants at various concentrations of **4**, $[\mathbf{4}] = (2.0$–$13.0) \times 10^{-4}$ M in MeCN at 263 K.

Fe···Fe distance than the μ-OAc one, being composed of three atoms. Thus, the diiron core of **2** might shrink compared with that of **1a**. The structure of the hexpy ligand might be suitable for the structural features of the diiron core in **2**. The tight encapsulation by the hexpy ligand is reflected in the smallest ν_{O-O} value of **2** as described above. The relatively higher energy μ-peroxo to Fe^{3+} charge-transfer band of **2** suggested that the Fe–O_{peroxo} bond is strengthened by the hexpy ligand. The thermal stability of **2** might be enhanced by tight encapsulation induced by the hexpy ligand.

To date, four peroxodiiron(III) complexes have been structurally characterized by X-ray analyses.[27–30] Suzuki et al. reported the most thermally stable peroxodiiron complex with a sterically hindered dinucleating ligand.[27] The diiron core is protected from attack by polar molecules such as water and solvents, and by steric hindrance of the many phenyl groups substituted at the imidazole donors of the dinucleating ligand. The hydrophobic pocket also assists reversible O_2-binding of the peroxodiiron complex. Que et al. reported the crystal structure of the thermally stable peroxodiiron(III) complex with a sterically hindered dinucleating ligand.[30] Lippard et al. reported the crystal structure of the peroxodiiron(III) complex originally studied by Kitajima et al.[29] This complex is not very stable at higher temperatures, although the ligand induces a large steric hindrance. It is likely that the steric hindrance of the ligand is essential for stabilization of the peroxodiiron complex as shown in Chart 1. **2** is very stable at room temperature although the hexpy ligand is markedly less sterically hindered than the ligands shown in Chart 1. Therefore, it is concluded that **2** is unique not only in terms of the triply bridged peroxodiiron core structure, but also in terms of the high thermal stability without steric hindrance of the ligand. Given its less sterically hindered structure, **2** might prove useful as a promising functional model of sMMO to investigate O_2-activation and oxygenation of external substrates.

Conclusion

Diiron complexes of the polypyridine ligands tripy and hexpy, $[Fe_2(O)(OAc)_2(hexpy)](CF_3SO_3)_2$ (**1c**) and $[Fe_2(O)(OAc)_2(tripy)_2](ClO_4)_2$ (**3**), were prepared and converted to the peroxodiiron complexes $[Fe_2(O)(O_2)(OAc)(hexpy)](CF_3SO_3)$ (**2**) and $[Fe_2(O)(O_2)(OAc)(tripy)_2](ClO_4)$ (**4**). The structural features of **2** and **4** were fully characterized by means of various spectroscopic studies. Both **2** and **4** possess a unique triply bridged μ-acetato-μ-oxo-μ-1,2-peroxodiiron core structure. The thermal stability of the peroxodiiron complexes and the spontaneous decomposition mechanism of **2** were investigated by kinetic methods and product analysis. The thermal stability of **2** is greatly enhanced by the hexpy ligand, which might act by tightly encapsulating the diiron core.

We thank Prof. T. Kitagawa, Institute for Molecular Science, and Prof. S. Hirota for the resonance Raman spectral studies, Prof. H. Ōkawa and M. Ohba, Kyushu University, for the magnetic measurements, and Dr. S. Iijima, National Institute in Tsukuba, for the Mössbauer spectral studies. This work was supported by a Grant-in-Aid for Scientific Research B (No. 14340210) from the Japan Society for the Promotion of Science.

References

1 E. I. Solomon, T. C. Brunold, M. I. Davis, J. N. Kemsley, S.-K. Lee, N. Lehnert, F. Neese, A. J. Skulan, Y.-S. Yang, J. Zhou, *Chem. Rev.* **2000**, *100*, 235.

2 *Handbook of Metalloproteins*, ed. by A. Messerschmidt, R. Huber, T. Poulos, K. Wieghardt, Wiley, New York, **2001**, Vol. 2.

3 R. E. Stenkamp, *Chem. Rev.* **1994**, *94*, 715.

4 T. C. Brunold, E. I. Solomon, *J. Am. Chem. Soc.* **1999**, *121*, 8277.

5 T. C. Brunold, E. I. Solomon, *J. Am. Chem. Soc.* **1999**, *121*, 8288.

6 M. Wirstam, S. J. Lippard, R. A. Friesner, *J. Am. Chem. Soc.* **2003**, *125*, 3980.

7 P. C. Wilkins, R. G. Wilkins, *Coord. Chem. Rev.* **1987**, *79*, 195.

8 M. A. Holmes, I. L. Trong, S. Turley, L. C. Sieker, R. E. Stenkamp, *J. Mol. Biol.* **1991**, *218*, 583.

9 J. L. Smith, W. A. Hendrickson, A. W. Addison, *Nature* **1983**, *303*, 86.

10 A. K. Shiemke, T. M. Loehr, J. Sanders-Loehr, *J. Am. Chem. Soc.* **1986**, *108*, 2437.

11 B. J. Wallar, J. D. Lipscomb, *Chem. Rev.* **1996**, *96*, 2625.

12 M. Kodera, K. Kano, T. Funabiki, *Nonheme Monooxygenases*, in *Oxygenases and Model Systems*, ed. by T. Funabiki, Kluwer Academic Publishers, **1997**, p. 283.

13 M.-H. Baik, M. Newcomb, R. A. Friesner, S. J. Lippard, *Chem. Rev.* **2003**, *103*, 2385.

14 B. J. Brazeau, R. N. Austin, C. Tarr, J. T. Groves, J. D. Lipscomb, *J. Am. Chem. Soc.* **2001**, *123*, 11831.

15 A. M. Valentine, S. S. Stahl, S. J. Lippard, *J. Am. Chem. Soc.* **1999**, *121*, 3876.

16 S. K. Lee, B. G. Fox, W. A. Froland, J. D. Lipscomb, E. Munck, *J. Am. Chem. Soc.* **1993**, *115*, 6450.

17 K. E. Liu, A. M. Valentine, D. Wang, B. H. Huynh, D. E. Edmondson, A. Salifoglou, S. J. Lippard, *J. Am. Chem. Soc.* **1995**, *117*, 10174.

18 A. C. Rosenzweig, H. Brandstetter, D. A. Whittington, P. Nordlund, S. J. Lippard, C. A. Frederick, *Proteins* **1997**, *29*, 141.

19 N. Elango, R. Radhakrishnan, W. A. Froland, B. J. Wallar, C. A. Earhart, J. D. Lipscomb, D. H. Ohlendorf, *Protein Sci.* **1997**, *6*, 556.

20 B. G. Fox, M. P. Hendrich, K. K. Surerus, K. K. Andersson, W. A. Froland, J. D. Lipscomb, E. Münck, *J. Am. Chem. Soc.* **1993**, *115*, 3688.

21 K. E. Liu, D. Wang, B. H. Huynh, D. E. Edmondson, A. Salifoglou, S. J. Lippard, *J. Am. Chem. Soc.* **1994**, *116*, 7465.

22 K. E. Liu, A. M. Valentine, D. Qiu, D. E. Edmondson, E. H. Appelman, T. G. Spiro, S. J. Lippard, *J. Am. Chem. Soc.* **1995**, *117*, 4997.

23 L. J. Shu, J. C. Nesheim, K. Kauffmann, E. Münck, J. D. Lipscomb, L. Que, Jr., *Science* **1997**, *275*, 515.

24 S. Pulver, W. A. Froland, B. G. Fox, J. D. Lipscomb, E. I. Solomon, *J. Am. Chem. Soc.* **1993**, *115*, 12409.

25 L. Que, Jr., Y. Dong, *Acc. Chem. Res.* **1996**, *29*, 190.

26 M. Kodera, Y. Taniike, M. Itoh, Y. Tanahashi, H. Shimakoshi, K. Kano, S. Hirota, S. Iijima, M. Ohba, H. Okawa, *Inorg. Chem.* **2001**, *40*, 4821.

27 T. Ookubo, H. Sugimoto, T. Nagayama, H. Masuda, T. Sato, K. Tanaka, Y. Maeda, H. Ōkawa, Y. Hayashi, A. Uehara, M. Suzuki, *J. Am. Chem. Soc.* **1996**, *118*, 701.

28 X. Zhang, H. Furutachi, S. Fujinami, S. Nagatomo, Y.

Maeda, Y. Watanabe, T. Kitagawa, M. Suzuki, *J. Am. Chem. Soc.* **2005**, *127*, 826.

29 K. Kim, S. J. Lippard, *J. Am. Chem. Soc.* **1996**, *118*, 4914.

30 Y. Dong, S. Yan, V. G. Young, L. Que, Jr., *Angew. Chem., Int. Ed. Engl.* **1996**, *35*, 618.

31 H. Sugimoto, T. Nagayama, S. Maruyama, S. Fujinami, Y. Yasuda, M. Suzuki, A. Uehara, *Bull. Chem. Soc. Jpn.* **1998**, *71*, 2267.

32 Y. Hayashi, T. Kayatani, H. Sugimoto, M. Suzuki, K. Inomata, A. Uehara, Y. Mizutani, T. Kitagawa, Y. Maeda, *J. Am. Chem. Soc.* **1995**, *117*, 11220.

33 Y. Dong, Y. Zang, L. Shu, E. C. Wilkinson, L. Que, Jr., *J. Am. Chem. Soc.* **1997**, *119*, 12683.

34 T. C. Brunold, N. Tamura, N. Kitajima, Y. Moro-oka, E. I. Solomon, *J. Am. Chem. Soc.* **1998**, *120*, 5674.

35 Y. Dong, S. Ménage, B. A. Brennan, T. E. Elgren, H. G. Jang, L. L. Pearce, L. Que, Jr., *J. Am. Chem. Soc.* **1993**, *115*, 1851.

36 S. V. Kryatov, S. Taktak, I. V. Korendovych, E. V. Rybak-Akimova, J. Kaizer, S. Torelli, X. Shan, S. Mandal, V. L. MacMurdo, A. Mairata i Payeras, L. Que, Jr., *Inorg. Chem.* **2005**, *44*, 85.

37 S. V. Kryatov, F. A. Chavez, A. M. Reynolds, E. V. Rybak-Akimova, L. Que, Jr., W. B. Tolman, *Inorg. Chem.* **2004**, *43*, 2141.

38 S. V. Kryatov, E. V. Rybak-Akimova, V. L. MacMurdo, L. Que, Jr., *Inorg. Chem.* **2001**, *40*, 2220.

39 M. Costas, C. W. Cady, S. V. Kryatov, M. Ray, M. J. Ryan, E. V. Rybak-Akimova, L. Que, Jr., *Inorg. Chem.* **2003**, *42*, 7519.

40 V. L. MacMurdo, H. Zheng, L. Que, Jr., *Inorg. Chem.* **2000**, *39*, 2254.

41 N. Kitajima, N. Tamura, H. Amagai, H. Fukui, Y. Moro-oka, Y. Mizutani, T. Kitagawa, R. Mathur, K. Heerwegh, C. A. Reed, C. R. Randall, L. Que, Jr., K. Tatsumi, *J. Am. Chem. Soc.* **1994**, *116*, 9071.

42 Y. Dong, H. Fujii, M. P. Hendrich, R. A. Leising, G. Pan, C. R. Randall, E. C. Wilkinson, Y. Zang, L. Que, Jr., B. G. Fox, K. Kauffmann, E. Münck, *J. Am. Chem. Soc.* **1995**, *117*, 2778.

43 H.-F. Hsu, Y. Dong, L. Shu, V. G. Young, Jr., L. Que, Jr., *J. Am. Chem. Soc.* **1999**, *121*, 5230.

44 H. Zheng, S. J. Yoo, E. Münck, L. Que, Jr., *J. Am. Chem. Soc.* **2000**, *122*, 3789.

45 J. Sanders-Loehr, W. D. Wheeler, A. K. Shiemke, B. A. Averill, T. M. Loehr, *J. Am. Chem. Soc.* **1989**, *111*, 8084.

46 J.-A. R. Hartman, R. L. Rardin, P. Chaudhuri, K. Pohl, K. Wieghardt, B. Nuber, J. Weiss, G. C. Papaefthymiou, R. B. Frankel, S. J. Lippard, *J. Am. Chem. Soc.* **1987**, *109*, 7387.

47 W. H. Armstrong, A. Spool, G. C. Papaefthymiou, R. B. Frankel, S. J. Lippard, *J. Am. Chem. Soc.* **1984**, *106*, 3653.

48 M. C. White, A. G. Doyle, E. N. Jacobsen, *J. Am. Chem. Soc.* **2001**, *123*, 7194.

49 K. Chen, M. Costas, J. Kim, A. K. Tipton, L. Que, Jr., *J. Am. Chem. Soc.* **2002**, *124*, 3026.

50 C. Kim, Y. Dong, L. Que, Jr., *J. Am. Chem. Soc.* **1997**, *119*, 3635.

51 J. B. Vincent, J. C. Huffman, G. Christou, *J. Am. Chem. Soc.* **1988**, *110*, 6898.

52 M. Kodera, H. Shimakoshi, K. Kano, *Chem. Commun.* **1996**, 1737.

53 J. Y. Ryu, J. Kim, M. Costas, K. Chen, W. Nam, L. Que, Jr., *Chem. Commun.* **2002**, 1288.

54 M. Itoh, J. Nakazawa, K. Maeda, K. Kano, T. Mizutani, M. Kodera, *Inorg. Chem.* **2005**, *44*, 691.

55 M. Kodera, H. Shimakoshi, M. Nishimura, H. Okawa, S. Iijima, K. Kano, *Inorg. Chem.* **1996**, *35*, 4967.

56 M. Kodera, H. Shimakoshi, Y. Tachi, K. Katayama, K. Kano, *Chem. Lett.* **1998**, 441.

57 M. Kodera, Y. Tachi, S. Hirota, K. Katayama, H. Shimakoshi, K. Kano, K. Fujisawa, Y. Moro-oka, Y. Naruta, T. Kitagawa, *Chem. Lett.* **1998**, 389.

58 A. J. Sitter, J. Terner, *J. Labelled Compd. Radiopharm.* **1984**, *22*, 461.

59 D. T. Cromer, J. T. Waber, *International Tables for X-ray Crystallography*, Kynoch Press, Birmingham, **1974**, Vol. 4.

60 J. A. Ibers, W. C. Hamilton, *Acta Crystallogr.* **1964**, *17*, 781.

61 D. C. Creagh, W. J. McAuley, *International Tables for X-ray Crystallography*, Kluwer, Boston, **1992**.

62 *Crystal Structure Analysis Package, Version 3.6*, Molecular Structure Corp. and Rigaku Corp., The Woodlands, TX, **2004**.

63 J.-A. R. Hartman, R. L. Rardin, P. Chaudhuri, K. Pohl, K. Wieghardt, B. Nuber, J. Weiss, G. C. Papaefthymiou, R. B. Frankel, S. J. Lippard, *J. Am. Chem. Soc.* **1987**, *109*, 7387.

64 W. H. Armstrong, A. Spool, G. C. Papaefthymiou, R. B. Frankel, S. J. Lippard, *J. Am. Chem. Soc.* **1984**, *106*, 3653.

65 HB(pz′) represents hydrotris(3,5-diisopropyl-1-pyrazolyl)-borate.